



Simultaneous Cr(VI) reduction and Cr(III) removal of bifunctional MOF/Titanate nanotube composites



Xun Wang ^a, Wen Liu ^b, Huifen Fu ^a, Xiao-Hong Yi ^a, Peng Wang ^a, Chen Zhao ^a, Chong-Chen Wang ^{a,*}, Weiwei Zheng ^c

^a Beijing Key Laboratory of Functional Materials for Building Structure and Environment Remediation/Beijing Advanced Innovation Centre for Future Urban Design, Beijing University of Civil Engineering and Architecture, Beijing 100044, China

^b The Key Laboratory of Water and Sediment Sciences, Ministry of Education, College of Environment Sciences and Engineering, Peking University, Beijing 100871, China

^c Department of Chemistry, Syracuse University, Syracuse, NY 13244, United States

ARTICLE INFO

Article history:

Received 30 January 2019

Received in revised form

13 March 2019

Accepted 23 March 2019

Available online 25 March 2019

Keywords:

BUC-21

Titanate nanotubes

Photocatalysis

Adsorption

Chromium

ABSTRACT:

In this study, a series of **BUC-21**/titanate nanotube (**BT-X**) composites were facilely fabricated via ball-milling of 2-dimensional (2D) metal-organic framework (MOF) **BUC-21** and titanate nanotubes (TNTs). The **BT-X** composites were characterized by powder X-ray diffraction (PXRD), Fourier transform infrared spectroscopy (FTIR), transmission electron microscopy (TEM), UV-visible diffuse-reflectance spectroscopy (UV-vis DRS), X-ray photoelectron spectrometer (XPS) and high resolution transmission electron microscopy (HRTEM). Both the photocatalytic reduction from Cr(VI) to Cr(III) and adsorptive removal of formed Cr(III) of **BT-X** composites were systematically investigated under different conditions including pH values and co-existing inorganic ions. It was found that **BUC-21** (100 mg)/TNTs (100 mg) (**BT-1**) composites demonstrate remarkable ability of photocatalytic Cr(VI) reduction and adsorptive Cr(III) removal, as well as good reusability and stability. It is believed that the introduction of TNTs could capture the formed Cr(III) from the surface of **BUC-21**, which provided more active sites exposed to enhance the Cr(VI) reduction.

© 2019 Elsevier Ltd. All rights reserved.

1. Introduction

Heavy metal contamination in water has been of great concern along with the development of rapid industrialization (Du et al., 2019a; Luo et al., 2019; Luo et al., 2015; Song et al., 2018; Zhao et al., 2009). For example, chromium (VI) ions, produced from leather tanning, electroplating, cement, mining, photography, smelting, etc., are highly toxic and pose great threat on the health of mankind by dermatitis, bronchitis, liver damage, ulcer formation and carcinogenic effects (Gu et al., 2013; Ren et al., 2014; Wang et al., 2016; Wang et al., 2015b; Xia et al., 2018). Unlike lead or cadmium, chromium exists primarily as both low-toxic form of Cr(III) and high toxic Cr(VI) in aqueous environment (Wang et al., 2019; Ye et al., 2018; Zhang et al., 2014). Therefore, before waste water are discharged to the environment, the concentration of chromium (VI) must be reduced (Qiu et al., 2014). Among all the

elimination technologies like precipitation, electro-reduction, chemical reduction, coagulation, ion exchange, reverse osmosis and electro-dialysis, the photocatalytic Cr(VI) reduction into Cr(III) is well-acknowledged as an effective Cr(VI) removal method (Kang et al., 2017; Lu et al., 2017; Qiu et al., 2018b; Wang et al., 2015a; Wu et al., 2017; Xia et al., 2018; Yuan et al., 2018; Zhang et al., 2018a; Zhang et al., 2018b; Zou et al., 2019). Photocatalysis, as a green and sustainable technology, displays some advantages in wastewater treatment: (i) mild work environment; (ii) possibly complete mineralization and (iii) low working cost (Nie et al., 2018; Wang et al., 2018; Wu et al., 2018a; Wu et al., 2018b; Wu et al., 2018c; Zou et al., 2016). Generally, the formed Cr(III) was further removed through precipitation to form Cr(OH)₃ by adding lime or NaOH, and the additional procedure always need complex equipment with increased cost. Therefore, it is highly desirable to develop a new strategy to simultaneously reduce Cr(VI) and remove Cr(III) with the aid of multi-functional materials.

Metal-organic frameworks (MOFs), a class of porous crystalline solids with infinite network structures built from organic linkers and

* Corresponding author.(C.-C. Wang).

E-mail address: wangchongchen@bucea.edu.cn (C.-C. Wang).

inorganic metal ions (Li et al., 2019; Qiu et al., 2018a; Xu et al., 2018a), have been recognized to be promising functional materials for diverse systems, including drug delivery (Wang et al., 2014; Xu et al., 2018b), catalysis (Wang et al., 2010; Wang et al., 2011), photocatalysis (Du et al., 2019a; Du et al., 2019b; Wang et al., 2016; Wang et al., 2017; Yi et al., 2019; Yi et al., 2018), gas storage (Yi et al., 2019; Zhao et al., 2016b), gas separation (Fu et al., 2018; Pi et al., 2017), adsorbents (Du et al., 2017a; Du et al., 2017b; Du et al., 2019b; Li et al., 2017; Liu et al., 2018; Li et al., 2017; Song et al., 2018; Ye et al., 2018). **BUC-21** was a chemically stable 2D MOF constructed from *cis*-1,3-dibenzyl-2-oxo-4,5-imidazolidinedicarboxylic acid as linker and Zn²⁺ as template, which exhibited superior photocatalytic performance toward Cr(VI) reduction under UV light irradiation (Wang et al., 2017).

Subsequently, the metal-free g-C₃N₄ was introduced to fabricate the g-C₃N₄/**BUC-21** composite photocatalyst, which exhibited the enhanced photocatalytic activities toward Cr(VI) under the simulated sunlight (Yi et al., 2019). Titanate nanotubes (TNTs) synthesized through hydrothermal methods is getting increased attentions due to the lower fabrication cost, large specific surface area, and large pore volumes from their nanotubular structure. Titanate nanotubes can be described as multi-walled spiral nanoscrolls formed by rolling of two-dimensional (2D) TiO₆ octahedral nanolayers, resulting in tubular structures with almost uniform inner diameters of ~5 nm and outer diameters of ~10 nm, while the length of TNTs can be several hundreds of nanometers (Bavykin and Walsh, 2009; Kukovecz et al., 2016). These structural features and the mobile

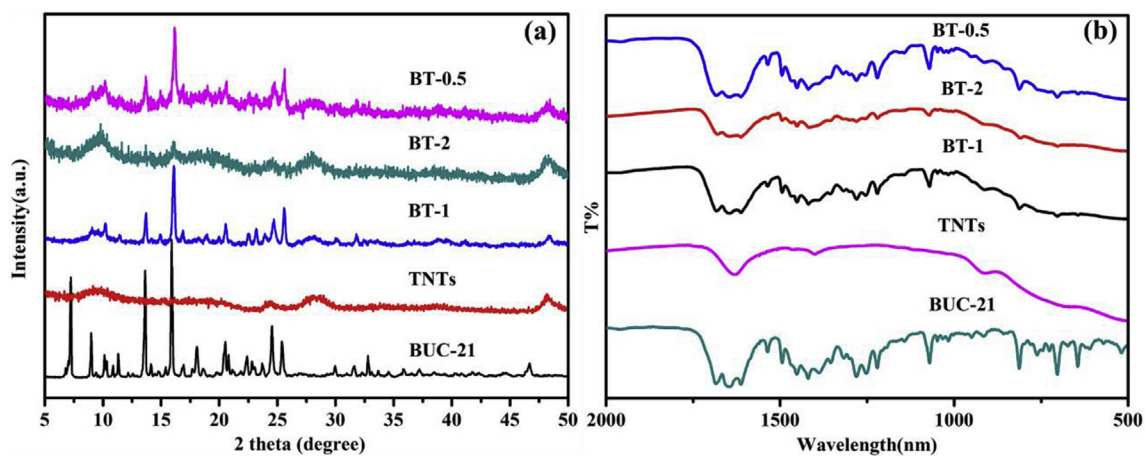


Fig. 1. (a) PXRD patterns of the **BUC-21**, TNTs and series **BT-X** composites. (b) FTIR spectra of the **BUC-21**, TNTs and series **BT-X** composites.

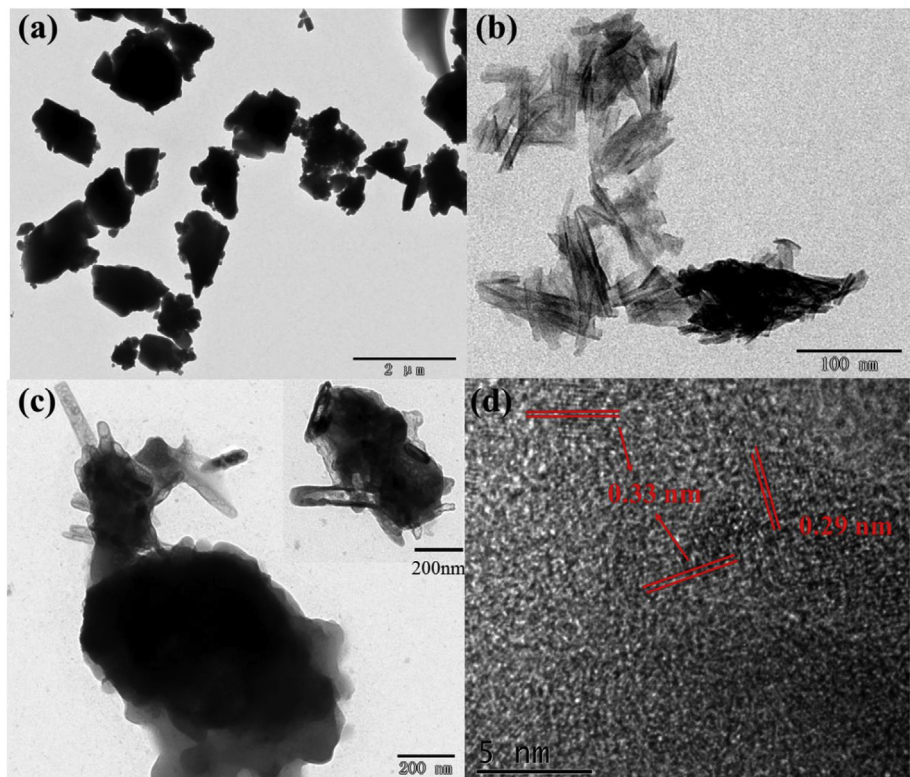


Fig. 2. TEM images of (a) pure **BUC-21**, (b) pure TNTs, (c) **BT-1**, and (d) HRTEM images of **BT-1**.

cations on the surface as well as between the titanate layers make the TNTs excellent ion-exchange media, which may be directly applied in e.g. the removal of hazard heavy metal ions in natural waters and promising candidate materials for dye-sensitized solar cells, photocatalysis, supercapacitors, and rechargeable lithium batteries (Gao et al., 2009; Liu et al., 2014; Liu et al., 2013a; Liu et al., 2016; Wang et al., 2013a; Zhao et al., 2016a). In this study, a series MOF/TNTs were facilely fabricated ball-milling of 2-dimensional (2D) metal-organic framework (MOF) **BUC-21** (Wang et al., 2017) and titanate nanotubes (TNTs). The comprehensive investigations under different conditions including pH values and co-existing inorganic ions indicate that the introduction of TNTs could capture the formed Cr(III)

accumulated on the surface of **BUC-21**, which provided more surface active sites to enhance the Cr(VI) reduction. Therefore, the **BUC-21**/TNTs composites display remarkable ability for both photocatalytic Cr(VI) reduction and adsorptive Cr(III) removal.

2. Experimental

2.1. Materials and instruments

All chemicals are commercially available with reagent grade and were used directly without further purification. Powder X-ray diffraction (PXRD) patterns were recorded in the range of $2\theta = 5^\circ -$

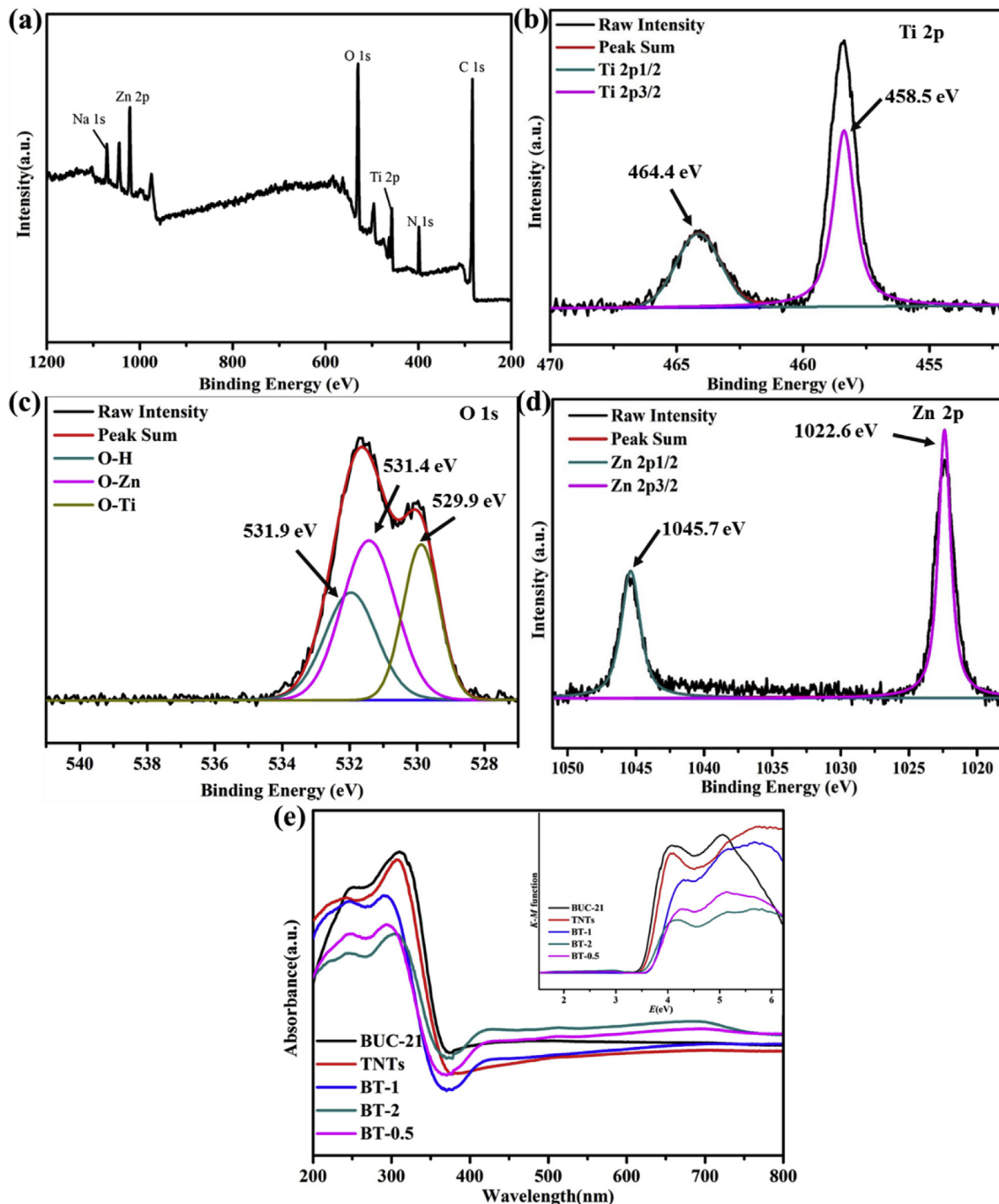


Fig. 3. (a) The XPS survey spectrum. (b) Ti 2p spectrum; (c) O 1s spectrum; (d) Zn 2p spectrum of **BT-1** composite; (e) UV–vis spectra and (inset) Kubelka-Munk-transformed diffuse reflectance spectrum of **BUC-21**, TNTs and **BT-X** composites.

50° on a DX-2700B X-ray diffractometer with Cu $\text{K}\alpha$ radiation. Fourier transform infrared (FTIR) spectra were recorded from 4000 cm^{-1} to 400 cm^{-1} on a Nicolet 6700 infrared spectrophotometer with KBr pellets. UV–Vis diffuse reflectance spectra (UV–Vis DRS) were measured between 200 nm and 800 nm on a PerkinElmer Lambda 650S spectrophotometer using BaSO_4 as the reference with 100% reflectance. The morphologies of the samples were studied on Tecnai G2 F20 S-TWIN (HRTEM) and JEM 1200EX transmission electron microscopy (TEM). X-ray photoelectron spectra (XPS) measurements were carried out on a Thermo ESCALAB 250XI. The zeta potentials of sample under different pH values were determined by a JS94H zeta potential analyzer at room temperature.

2.2. Preparation of BUC-21/TNTs composites

BUC-21 was hydrothermally synthesized according to the previous report (Wang et al., 2017). Briefly, a mixture of 0.3 mmol ZnCl_2 , 0.3 mmol 4,4-bipyridine and 0.3 mmol *cis*-1,3-dibenzyl-2-oxo-4,5-imidazolidinedicarboxylic acid were sealed in a 25 mL Teflon-lined stainless steel Parr bomb containing 18 mL deionized H_2O , and heated at 160 °C for 72 h.

Titanate nanotubes (TNTs) were prepared by a hydrothermal method using commercial P25 TiO_2 as precursor (Liu et al., 2014). Briefly, the suspension of 0.3 g TiO_2 in 16.5 mL 10 M NaOH solution were autoclaved at 130 °C in a 25 mL Teflon-lined stainless steel Parr bomb for 72 h. The TNTs were separated via filtration and washed with deionized water until the leachate to neutral.

The **BUC-21**/TNTs composites were prepared via ball-milling of the mixture of as-prepared **BUC-21** and TNTs at 30 Hz for 40 min. A

series of **BUC-21**/TNTs composites were prepared with different mass content of **BUC-21** and TNTs, which were donated as **BT-0.5** (100 mg **BUC-21**, 50 mg TNTs), **BT-1** (100 mg **BUC-21**, 100 mg TNTs) and **BT-2** (100 mg **BUC-21**, 200 mg TNTs), respectively.

2.3. Photocatalysis and adsorption activity

Both photocatalysis and adsorption experiments were conducted in a 300 mL quartz reactor containing 250 mL $\text{K}_2\text{Cr}_2\text{O}_7$ aqueous solution (10 mg L^{-1}) and 40.0 mg **BT-X** composite. After stirring for 60 min to reach adsorption – desorption equilibrium, the suspensions were irradiated by a 500-W Hg lamp (Beijing Aulight Co., Ltd). The spectrum of the Hg lamp was shown in Fig. S1. During the photocatalytic experiments, 2.5 mL suspension was extracted by a 0.22 μm filter at 10 min intervals for further analysis. The concentration of Cr(VI) was determined by a dinitrophenyl carbazide spectrophotometric method at 540 nm on a Laspec Alpha-1860 spectrometer (Athanasenou et al., 2016). The total Cr concentration was measured by Flame Atomic Absorption Spectrometry (AAS, PinAAcle 900T, Perkin-Elmer, USA). The Cr(III) concentration was calculated as the difference between the concentration of total Cr and Cr(VI). The solution pH values were adjusted from 2.0 to 9.0 by using diluted H_2SO_4 and NaOH solutions, respectively.

3. Results and discussion

3.1. Characterizations

The powder X-ray diffraction patterns of the different materials

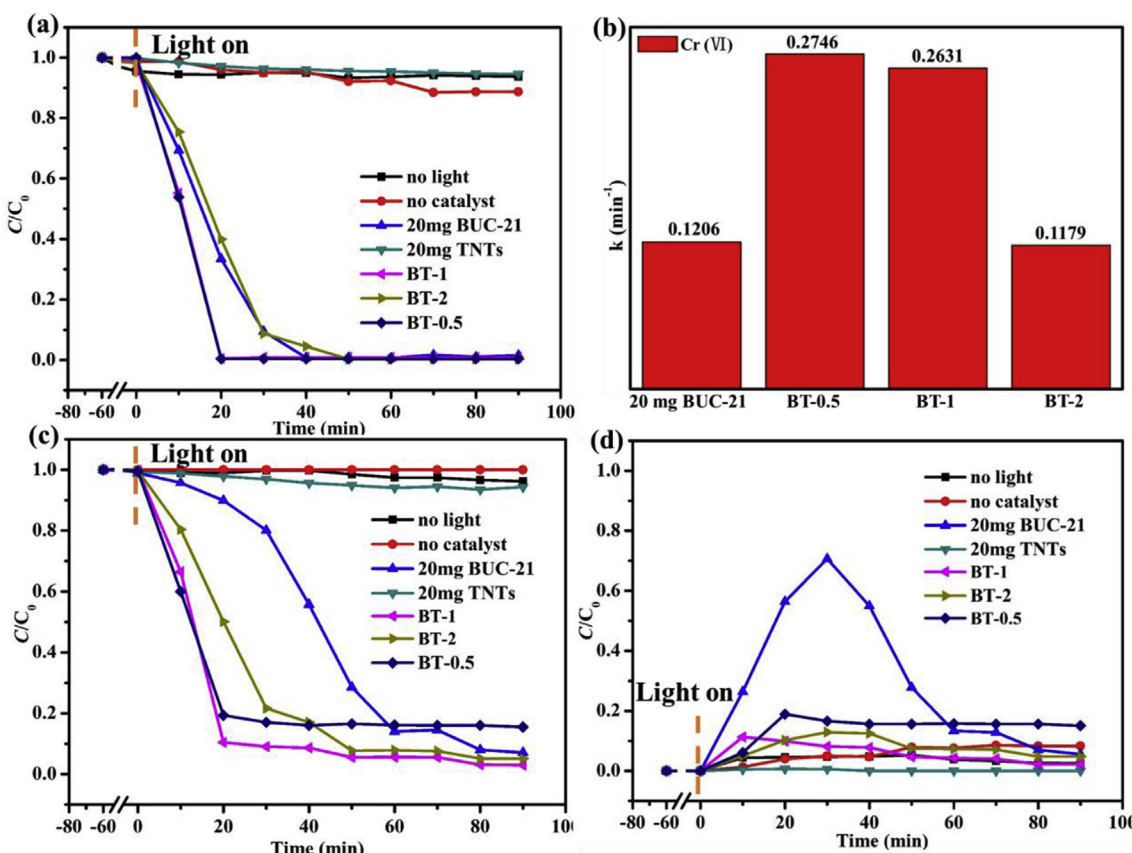


Fig. 4. (a) Photocatalytic Cr(VI) reduction efficiencies and (b) the corresponding reaction rate constants (k) of control experiments and in the presence of different photocatalysts. (c) The total Cr removal efficiencies of control experiments and in the presence of different photocatalysts. (d) Cr(III) removal efficiencies of control experiments and in the presence of different photocatalysts. Reaction conditions: 250 mL, Cr(VI) 10 mg L^{-1} , pH = 5, photocatalyst dosage 0.16 g L^{-1} .

are illustrated in Fig. 1a, in which the peaks at 10.2° , 13.6° , 14.8° , 15.9° , 20.5° , 24.5° and 25.5° of all **BT-X** composites can be assigned to the characteristics peaks of pure **BUC-21** (Wang et al., 2017; Yi et al., 2019). In addition, the peaks at 10° , 24° , 28° and 48° are contributed to the characteristics peaks of the pure TNTs, and the intense peak at 10° was ascribed to interlayer space of TNTs (Xiong et al., 2010). For comparison, both pristine **BUC-21** and TNTs were characterized by PXRD before and after ball milling. No significant change of the main characteristic PXRD peaks of **BUC-21** and TNTs was observed after ball milling (Fig. S2). In addition, no PXRD peaks of anatase or rutile were observed in TNTs after ball milling, indicating no phase change of the TNTs during the ball milling (Zhao et al., 2016a). The successful fabrication of **BT-X** composites can be further confirmed by their FTIR spectra as displayed in Fig. 1b (Yi et al., 2018). The strong and broad bands at 1645 and 1417 cm^{-1} were ascribed to the asymmetric and symmetric vibrations of carboxyl groups, respectively, and the bands at 1220 and 1141 cm^{-1} were assigned to the $\nu(\text{C}-\text{N})$ vibrations of the phenyl rings in **BUC-21**. For the pristine TNTs (Fig. 8a), the peaks at 1633 cm^{-1} and 466 cm^{-1} were contributed to the $\text{H}-\text{O}-\text{H}$ (bond water molecule) (Wang et al., 2013c) and the $\text{Ti}-\text{O}$ vibration in $[\text{Ti}-\text{O}_6]$ octahedrons (Xiong et al., 2011).

The pristine **BUC-21** exhibited agglomerated particle with relatively smooth surface (Fig. S3a), and the pure TNTs presented as long and hollow tubular structure (Fig. S3b). However, it was difficult to clearly identify the interaction between **BUC-21** and TNTs in **BT-1** composite from SEM image (Figs. S3c and S3d). Therefore, the successful fabrication of **BT-X** composites was further verified by TEM (Fig. 2a, b, 2c and Fig. S4), high-resolution TEM (Fig. 2d). As shown in Fig. 2a, the original **BUC-21** presented

as the aggregated particles with particle size ranging from 50 nm to 100 nm . The hollow, open-ended nanotubular structure of TNTs can be observed in Fig. 2b. The **BT-1** composites show irregular block of **BUC-21** and nanotubular structure of TNTs (Fig. 2c), in which the TNTs with the outer diameter of ca. 9 nm and tube length ranging from 50 to 300 nm were distributed with random orientation on the surface of **BUC-21**. The interactions between TNTs and **BUC-21** could be further affirmed by TEM profile image and HRTEM observation. It could be observed from the TEM section image (Fig. S4) that TNTs are uniformly distributed on the surface of **BUC-21**. As well, the HRTEM image (Fig. 2d) revealed that the measurement of the d spacing along the tube axis gives a value of 3.3 \AA , corresponding to the d spacing of the (010) planes in TNTs, and the d spacing along the direction perpendicular to the tube axis is about 2.9 \AA , close to the value of the (003) planes in TNTs (Fei et al., 2017; Thorne et al., 2005). Finally, the N_2 adsorption experiments demonstrated that BET surface area increased from $1.10\text{ m}^2\text{ g}^{-1}$ for **BUC-21** to $7.85\text{ m}^2\text{ g}^{-1}$ for **BT-1** (Table S1), which further confirmed the successfully combination between the **BUC-21** and TNTs. The increase of specific surface area was beneficial to expose more active sites to promote the reduction of Cr(VI) and adsorption of Cr(III) on composites.

The characteristic signals of C, N, O, Zn and Ti elements were presented in the XPS survey spectrum of **BT-1** composite (Fig. 3a), further confirming the successful combination of **BUC-21** and TNTs. The peaks at 458.5 and 464.4 eV (Fig. 3b) can be assigned to $\text{Ti} 2p_{3/2}$ and $\text{Ti} 2p_{1/2}$, respectively (Barrocas et al., 2017; Wu et al., 2015). The peaks at 529.9 eV , 531.4 eV and 531.9 eV of $\text{O} 1s$ (Fig. 3c) in **BT-1** could be contributed to $\text{O}-\text{Ti}$, $\text{O}-\text{Zn}$ and $\text{O}-\text{H}$, respectively (Salleem et al., 2017). The peaks at 1022.6 eV and 1045.7 eV (Fig. 3d)

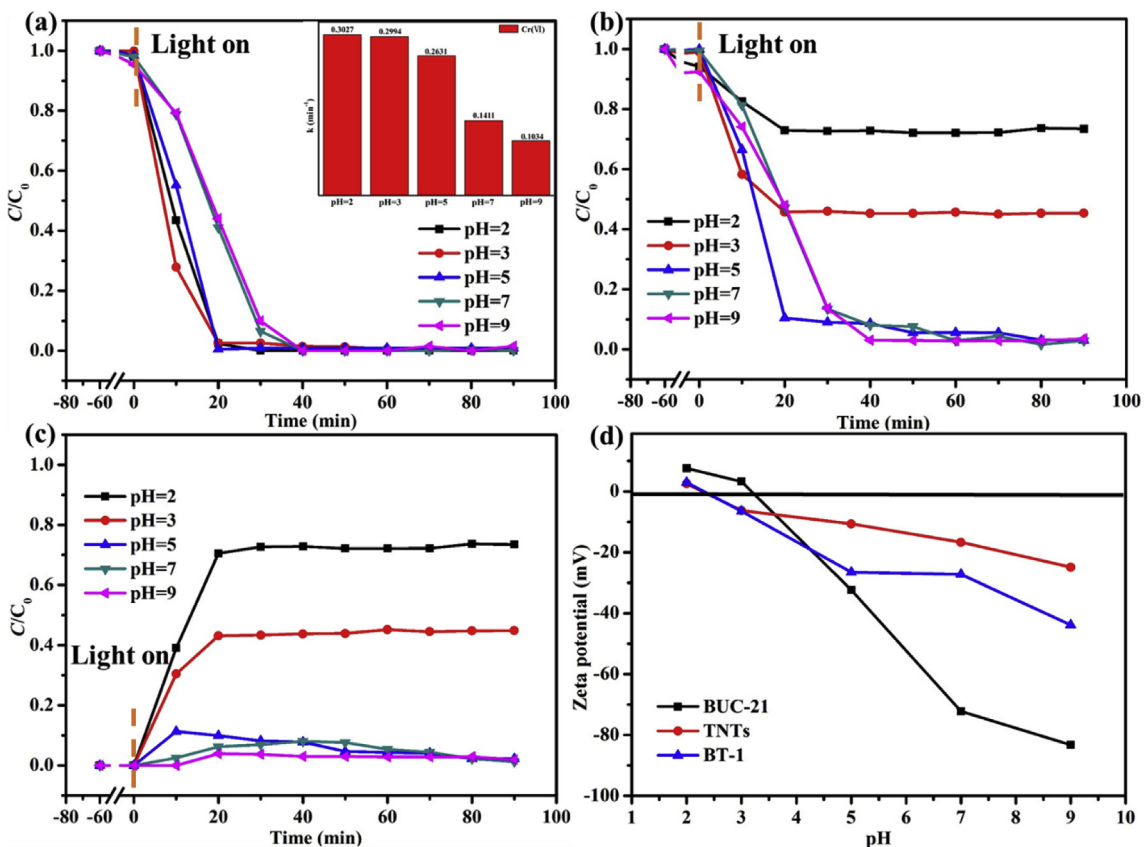


Fig. 5. (a) Reduction of Cr(VI) under UV light irradiation at different pH. (b) Removal of total Cr under UV light irradiation at different pH. (c) Removal of Cr(III) under UV light irradiation at different pH. (d) Zeta potentials of **BUC-21**, TNTs and **BT-1** at different pH. Reaction conditions: 250 mL , $\text{Cr(VI)} 10\text{ mg L}^{-1}$, $\text{pH}=5$, **BT-1** dosage 0.16 g L^{-1} .

corresponded to Zn 2p3/2 and Zn 2p1/2 (Abidli et al., 2015; Zhang et al., 2013), demonstrating the presence of Zn in the **BT-1** composite.

The UV–Vis absorption measurements indicate that the **BT-X** composites have a slightly blue-shifted absorption compared with that of the pristine **BUC-21** and TNTs (Fig. 3e). The band gap (E_g) of the samples were estimated using the Kubelka – Munk function, $F = (1-R)^2/2R$, where R is the reflectance of an infinitely thick layer at a given wavelength (Barrocas et al., 2016). The E_g values of **BT-1**, **BT-2** and **BT-0.5** are 3.73 eV, 3.62 eV and 3.73 eV, respectively, indicating that the **BT-X** composites might exhibit photocatalytic performances under the UV light irradiation.

3.2. Photocatalytic Cr(VI) reduction and adsorptive removal of Cr(III)

The photocatalytic activities of the prepared **BT-X** for Cr(VI) reduction and the adsorptive removal efficiencies for Cr(III) were evaluated under UV light irradiation. The experiment results, as depicted in Fig. 4a, revealed that the absence of light or catalysts led to nearly no Cr(VI) concentration decrease, while the presence of both light and catalysts like **BUC-21** and **BT-X** led to significant decrease in Cr(VI) concentration, indicating the photocatalytic reduction process for the Cr(VI) ions. The photocatalytic performance of **BT-X** composites with difference mass content of **BUC-21** and TNTs were also investigated. It was found that both **BT-0.5** and **BT-1** displayed similarly efficient Cr(VI) reduction (100% removal

within 20 min), which were superior to **BUC-21** (66.6% within 20 min, 100% within 40 min) and **BT-2** (60.1% within 20 min, 100% within 50 min). For the total Cr removal, **BT-1** exhibited the highest performance (89.6% at 20 min, and 97.6% within 90 min), followed by **BT-2** (92.3% at 50 min, and 95.0% within 90 min), **BT-0.5** (80.7% at 20 min, and 84.5% within 90 min) and **BUC-21** (86.0% at 60 min, and 92.9% within 90 min), as illustrated in Fig. 4b. It seems that pristine **BUC-21** in the composites could achieve good photocatalytic Cr(VI) reduction. However, if the formed Cr(III) ions failed to be transferred into TNTs, the accumulated Cr(III) would be precipitated into Cr(OH)_3 ($K_{\text{sp}} = 6.3 \times 10^{-31}$) under pH 5.0. The formed Cr(OH)_3 would cover the active sites of **BUC-21** photocatalyst, which resulted into the low removal performance (Fig. 4c). On the other hand, large proportion of TNTs in the composite like **BT-2** would decrease its photocatalytic activity, which also led to decreased total Cr removal. The enhanced Cr(VI) reduction and total Cr removal of **BT-1** can be contributed to synergetic effect of **BUC-21**'s photocatalytic Cr(VI) reduction and outstanding adsorption activity of TNTs. Therefore, the formed Cr(III) ions were transferred from the surface of **BUC-21** into TNTs, which reduced the local Cr(III) concentration and avoided the formation of Cr(OH)_3 precipitates to accomplish quick and efficient Cr removal. It should be noted that the removal efficiency of total Cr and Cr(VI) by pristine **BUC-21** and TNTs after ball milling displayed noticeable decrease (Fig. S5). However, the photocatalytic performances of **BT-X** composites are greatly improved compared to that of **BUC-21** and TNTs, implying that the introduction of TNTs can enhance the Cr(VI) removal efficiency.

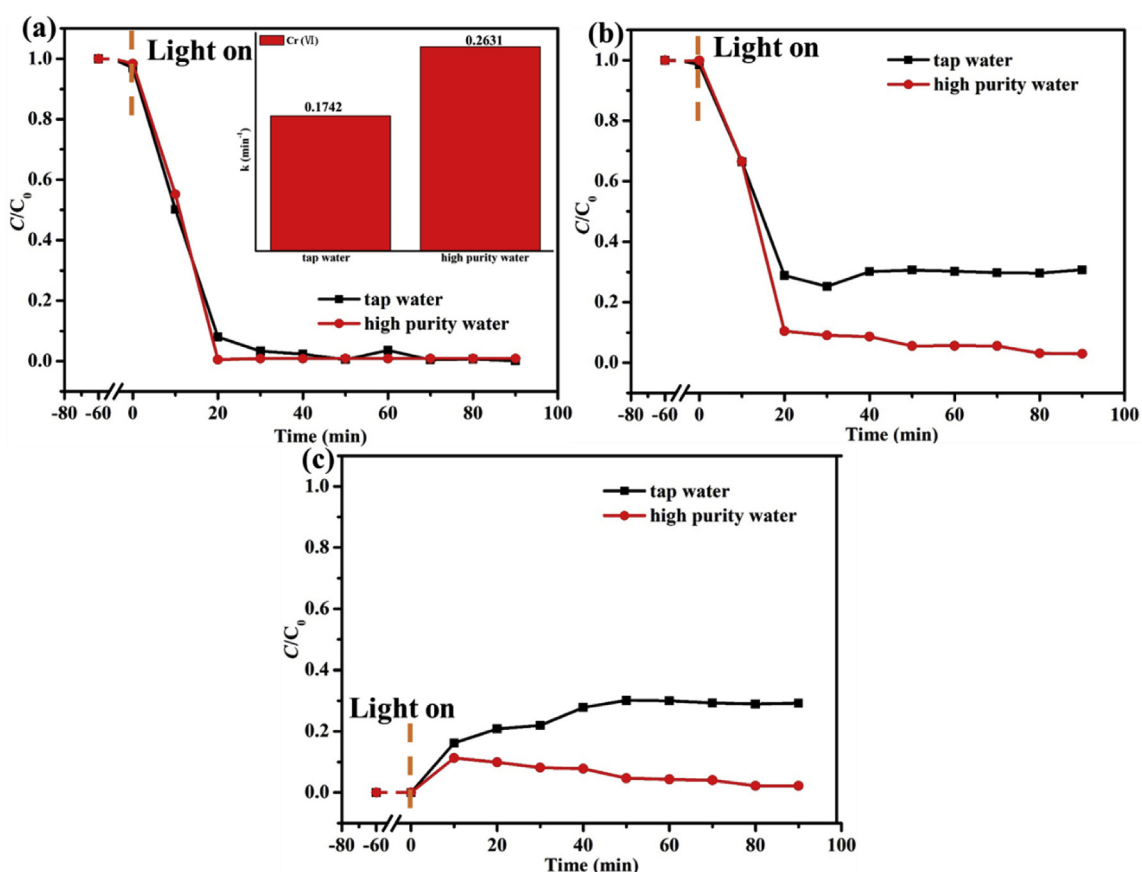
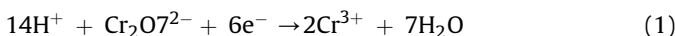


Fig. 6. (a) Reduction of Cr(VI), (b) removal of total Cr, (c) removal of Cr(III) over **BT-1** under UV light irradiation. The concentration of common ions in tap water: K^+ (3.6 mg L^{-1}), Na^+ (26.7 mg L^{-1}), Ca^{2+} (85.6 mg L^{-1}), Mg^{2+} (32.2 mg L^{-1}), Cl^- (58.6 mg L^{-1}), NO_3^- (9.5 mg L^{-1}), SO_4^{2-} (76.3 mg L^{-1}). Reaction conditions: 250 mL, 10 mg L^{-1} Cr(VI), $\text{pH} = 5$, **BT-1** = 0.16 g L^{-1} .

3.2.1. The influence of solution pH

The pH value of the reaction solution played significant role in both photocatalytic Cr(VI) reduction and Cr(III) adsorption (Liu et al., 2014). The acid conditions ($\text{pH} = 2, 3$ and 5) could promote the photocatalytic Cr(VI) reduction of **BT-1**, with reduction efficiency of nearly 100% in 20 min (Fig. 5a). Under the acidic conditions, the photocatalytic Cr(VI) reduction reaction occurred following the reaction as listed in Equations (1) and (2) (Zhao et al., 2014), in which the abundant H^+ could facilitate the photocatalytic process (as affirmed by the reaction rate constants in inset of Fig. 5a). With the increase of pH (7 and 9), the Cr(VI) reduction rates declined obviously, in which the 100% Cr(VI) reduction was achieved up to 40 min. In alkaline medium, CrO_4^{2-} was generally the main species of Cr(VI), and the reaction proceeded as Equations (2) and (3) (Wang et al., 2015a).



The total Cr removal efficiency with different pH values (Fig. 5b) revealed that pH 5.0 was an optimal condition, due to inhibiting photocatalytic Cr(VI) reduction under higher pH conditions (Fig. 5a) and lower pH (2.0) decreased the adsorption activities of TNTs toward Cr(III) (Fig. 5c). In detail, the adsorption of Cr(III) on **BT-1** was minor at lower pH due to low point of zero charge ($\text{pH}_{\text{PZC}} = 2.23$)

(Fig. 5d). As pH increased, more Cr(III) could be adsorbed onto the negatively charged surface of **BT-1** with the aid of electrostatic force and ion exchange with H^+/Na^+ in TNTs. When pH increased to optimal 5, the maximal removal efficiency of total Cr could reach 90.0% within 20 min. While, as solution pH further increased, Cr(III) could be precipitated as Cr(OH)_3 .

3.2.2. The influence of co-existing inorganic ions

Our previous research results revealed that the co-existing inorganic ions exerted minor influences on the photocatalytic Cr(VI) reduction performances of **BUC-21** (Wang et al., 2017; Yi et al., 2019). In order to explore the practical application, the Cr(VI) aqueous solutions prepared with tap water were photocatalytically treated with **BT-1** as photocatalyst under UV light irradiation. The co-existing inorganic ions including K^+ , Na^+ , Ca^{2+} , Mg^{2+} , Cl^- , NO_3^- and SO_4^{2-} exhibited minor impact on the photocatalytic activity of **BT-1**, which was confirmed by the Cr(VI) reduction efficiencies of 100% and 96% at 20 min of pure water solution and tap water solution, respectively. If the reaction time extended to 90 min, the photocatalytic Cr(VI) reduction efficiencies were identical for pure water solution and tap water solution (Fig. 6a). While, the co-existing inorganic ions might affect the adsorption process of TNTs (Liu et al., 2014; Liu et al., 2013b; Wang et al., 2013b). It was reported that the inhibition of inorganic ions on the adsorption activity of TNTs followed the order of $\text{Na}^+ \approx \text{K}^+ \ll \text{Mg}^{2+} < \text{Ca}^{2+}$ (Liu et al., 2013b). From Fig. 6c, it was found that the inorganic ions in the tap water exerted significant impact on the Cr(III) adsorption behavior onto TNTs, which subsequently

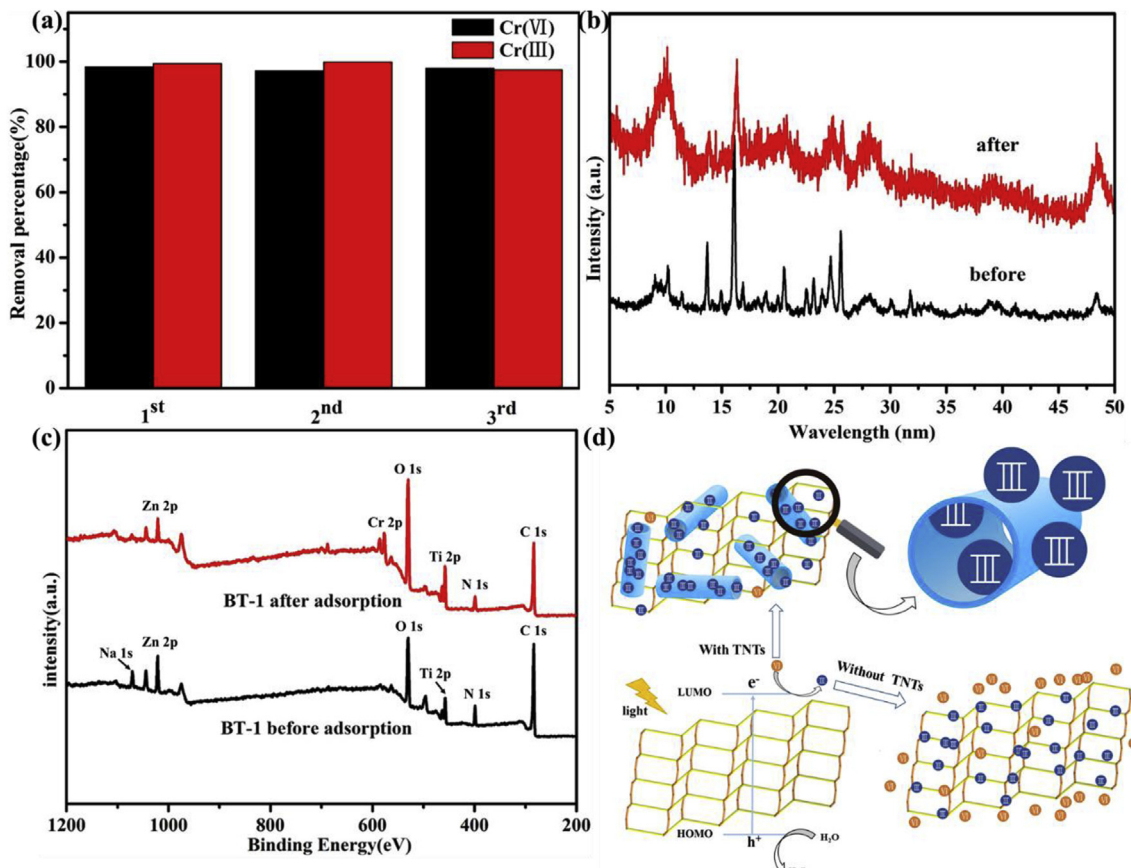


Fig. 7. (a) The reusability of **BT-1** for the removal of Cr(VI) and Cr(III). (b) PXRD patterns of **BT-1** before and after three recycles for Cr removal. (c) The XPS survey scan spectra for **BT-1** before and after photocatalysis-adsorption process. (d) A proposed possible reaction mechanism of photocatalysis and adsorption with **BT-1**. Reaction conditions: 250 mL, Cr(VI) 10 mg L⁻¹, pH = 5, **BT-1** dosage 0.16 g L⁻¹.

inhibited the total Cr removal (Fig. 6b). Although the noticeable negative impact of co-existing inorganic ions was found on the total Cr removal, it was feasible to utilize **BT-1** to perform photocatalysis-adsorption treatment of Cr(VI) with 72.0% removal efficiency in short reaction time (20 min).

3.2.3. Reusability and stability of **BT-1**

The reusability and stability of **BT-1** photocatalyst is essential for its potential practical applications. It was found that the photocatalytic Cr(VI) reduction and Cr(III) removal efficiencies of **BT-1** displayed no obvious decrease after three successive runs without any post-treatment (Fig. 7a), indicating that **BT-1** was highly stable and could be used repeatedly for Cr pollution treatment. Furthermore, no phase change was observed from the PXRD patterns of **BT-1** before and after photocatalysis/adsorption reaction (Fig. 7b), demonstrating the good structure and phrase stability of **BT-1** composite.

3.2.4. Photocatalysis and adsorption mechanism of **BT-1**

In our previous work (Wang et al., 2017), it was found that electrons are moved from the highest occupied molecular orbital (HOMO) of **BUC-21** to its lowest unoccupied molecular orbital (LUMO), and the holes (h^+) are accumulated in HOMO under UV light irradiation. The photo-induced electrons in the LUMO are usually easily lost to reduce Cr(VI) to Cr(III) (Dias and Petit, 2015; Gao et al., 2017) and H_2O accepted holes in absence of reducing agents (Liu et al., 2014). As shown in Fig. 7(d), the formed Cr(III) can be accumulated around **BUC-21** via their electrostatic interactions, which can inhibit further Cr(VI) reduction due to the high local concentration of Cr(III) and even the formation of Cr(OH)_3 precipitates on the surface of **BUC-21**. The introduction of TNTs in **BT-1** composite led to an efficient Cr(III) adsorption owing to both ion-exchange with H^+/Na^+ (Fig. 7c) and electrostatic attractions (Liu et al., 2014). The ion-exchange with H^+/Na^+ was further confirmed by XPS determination (Fig. 7c) and EDS mapping (Fig. S3e and Fig. S3f), in which the Na content decreased significantly. The transfer of Cr(III) from the surface of **BUC-21** to TNTs resulted in continuous release of more photocatalytic sites of **BUC-21** and the decrease of local Cr(III) concentration, which enhanced photocatalytic Cr(VI) reduction (Liu et al., 2014).

Consequently, the synergistic effect between **BUC-21** and TNTs can facilitate the total Cr removal resulted from the enhanced photocatalytic Cr(VI) reduction and adsorption toward Cr(VI).

4. Conclusions

The MOF photocatalyst/TNTs adsorbent composites (**BUC-21**/TNTs, **BT-X**) were facilely prepared via ball milling, which can achieve simultaneous Cr(VI) reduction and removal of Cr(III). The presence of TNTs can capture the formed Cr(III) on the **BUC-21** photocatalyst surface, reduce local Cr(III) concentration, eliminate possible Cr(OH)_3 precipitate, and therefore promotes the photocatalytic Cr(VI) reduction. The **BT-1** composite can be potentially used to treat Cr-containing wastewater due to: (1) its outstanding total Cr removal efficiency under weak acid condition ($\text{pH} = 5.0$); (2) the co-existing inorganic ions from real tap water exerting negligible influence on **BT-1**'s activity; (3) **BT-1** possess good stability and reusability after several runs. This work provides a flexible strategy to develop low-cost and highly effective MOF photocatalyst/adsorbent composite aiming to accomplish photocatalytic Cr(VI) reduction and further adsorptive removal of Cr(III). Further work is undergoing to combine visible light responsive MOFs like MIL-100(Fe), UiO-66-NH₂, MIL-125-NH₂ with TNTs, to achieve Cr(VI) removal under visible light or even sunlight.

Acknowledgements

This work was supported by National Natural Science Foundation of China (51878023, 51578034), Great Wall Scholars Training Program Project of Beijing Municipality Universities (CIT&TCD20180323), Project of Construction of Innovation Teams and Teacher Career Development for Universities and Colleges Under Beijing Municipality (IDHT20170508), Beijing Talent Project (2018A35), the Fundamental Research Funds for Beijing Universities (X18075/X18076/X18124/X18125/X18276) and Scientific Research Foundation of Beijing University of Civil Engineering and Architecture (KYJJ2017033/KYJJ2017008).

Appendix A. Supplementary data

Supplementary data to this article can be found online at <https://doi.org/10.1016/j.envpol.2019.03.096>.

References

- Abidli, A., Hamoudi, S., Belkacemi, K., 2015. Synthesis, characterization and insights into stable and well organized hexagonal mesoporous zinc-doped alumina as promising metathesis catalysts carrier. *Dalton Trans.* 44, 9823–9838.
- Athanasekou, C., Romanos, G.E., Papageorgiou, S.K., Manolis, G.K., Katsaros, F., Falaras, P., 2016. Photocatalytic degradation of hexavalent chromium emerging contaminant via advanced titanium dioxide nanostructures. *Chem. Eng. J.* 318, 171–180.
- Barrocas, B., Neves, M., Oliveira, M.C., Monteiro, O.C., 2017. Enhanced photocatalytic degradation of psychoactive substances using amine modified elongated titanate nanostructures. *Environ. Sci.: Nano* 5, 350–361.
- Barrocas, B., Silvestre, A.J., Rolo, A.G., Monteiro, O.C., 2016. The effect of ionic Co presence on the structural, optical and photocatalytic properties of modified cobalt-titanate nanotubes. *Phys. Chem. Chem. Phys.* 18, 18081.
- Bavykin, D.V., Walsh, F.C., 2009. Titanate and Titania Nanotubes.
- Dias, E.M., Petit, C., 2015. Towards the use of metal–organic frameworks for water reuse: a review of the recent advances in the field of organic pollutants removal and degradation and the next steps in the field. *J. Mater. Chem. 3*, 22484–22506.
- Du, X.-D., Wang, C.-C., Liu, J.-G., Zhao, X.-D., Zhong, J., Li, Y.-X., Li, J., Wang, P., 2017a. Extensive and selective adsorption of ZIF-67 towards organic dyes: performance and mechanism. *J. Colloid Interface Sci.* 506, 437–441.
- Du, X.D., Wang, C.C., Liu, J.G., Zhao, X.D., Zhong, J., Li, Y.X., Li, J., Wang, P., 2017b. Extensive and selective adsorption of ZIF-67 towards organic dyes: performance and mechanism. *J. Colloid Interface Sci.* 506, 437–441.
- Du, X.D., Yi, X.-H., Wang, P., Zheng, W., Deng, J., Wang, C.-C., 2019a. Robust photocatalytic reduction of Cr(VI) on UiO-66-NH₂(Zr/Hf) metal–organic framework membrane under sunlight irradiation. *Chem. Eng. J.* 356, 393–399.
- Du, X.D., Yi, X., Wang, P., Deng, J., Wang, C.-c., 2019b. Enhanced photocatalytic Cr(VI) reduction and diclofenac sodium degradation under simulated sunlight irradiation over MIL-100(Fe)/g-C₃N₄ heterojunctions. *Chin. J. Catal.* 40, 70–79.
- Fei, L.F., Lu, W., Hu, Y., Gao, G., Yong, Z., Sun, T., Zhou, N., Gu, H., Wang, Y., 2017. Evidencing the structural conversion of hydrothermal-synthesized titanate nanorod by in-situ electron microscopy. *J. Mater. Chem. 5*, 3786–3791.
- Fu, H., Wang, X., Wang, P., Wang, P., Wang, C.C., 2018. Enhanced acetone sensing performance of Au nanoparticle modified porous tube-like ZnO derived from rod-like ZIF-L. *Dalton Trans.* 47, 9014–9020.
- Gao, C., Wang, J., Xu, H., Xiong, Y., 2017. Coordination chemistry in the design of heterogeneous photocatalysts. *Chem. Soc. Rev.* 46, 2799–2823.
- Gao, T., Fjeld, H., Fjellvåg, H., Norby, T., Norby, P., 2009. In situ studies of structural stability and proton conductivity of titanate nanotubes. *Energy Environ. Sci.* 2, 517–523.
- Gu, H., Rapole, S.B., Huang, Y., Cao, D., Luo, Z., Wei, S., Guo, Z., 2013. Synergistic interactions between multi-walled carbon nanotubes and toxic hexavalent chromium. *J. Mater. Chem. 1*, 2011–2021.
- Kang, S., Wang, G., Zhao, H., Cai, W., 2017. Highly efficient removal of hexavalent chromium in aqueous solutions via chemical reduction of plate-like micro/nanostructured zero valent iron. *RSC Adv.* 7, 55905–55911.
- Kukovecz, Á., Kordás, K., Kiss, J., Kónya, Z., 2016. Atomic scale characterization and surface chemistry of metal modified titanate nanotubes and nanowires. *Surf. Sci. Rep.* 71, 473–546.
- Li, F., Wang, D., Xing, Q.J., Zhou, G., Liu, S.S., Li, Y., Zheng, L.L., Ye, P., Zou, J.P., 2019. Design and syntheses of MOF/COF hybrid materials via postsynthetic covalent modification: an efficient strategy to boost the visible-light-driven photocatalytic performance. *Appl. Catal. B Environ.* 243, 621–628.
- Li, J.J., Wang, C.C., Fu, H.F., Cui, J.R., Xu, P., Guo, J., Li, J.R., 2017. High-performance adsorption and separation of anionic dyes in water using a chemically stable graphene-like metal–organic framework. *Dalton Trans.* 46, 10197–10201.
- Liu, A., Wang, C.-C., Wang, C.-z., Fu, H.-f., Peng, W., Cao, Y.-L., Chu, H.-Y., Du, A.-F., 2018. Selective adsorption activities toward organic dyes and antibacterial

- performance of silver-based coordination polymers. *J. Colloid Interface Sci.* 512, 730–739.
- Liu, W., Jinren, N., Xiaochen, Y., 2014. Synergy of photocatalysis and adsorption for simultaneous removal of Cr(VI) and Cr(III) with TiO₂ and titanate nanotubes. *Water Res.* 53, 12–25.
- Liu, W., Sun, W., Borthwick, A.G.L., Ni, J., 2013a. Comparison on aggregation and sedimentation of titanium dioxide, titanate nanotubes and titanate nanotubes-TiO₂: influence of pH, ionic strength and natural organic matter. *Colloids Surf., A* 434, 319–328.
- Liu, W., Wang, T., Borthwick, A.G.L., Wang, Y., Yin, X., Li, X., Ni, J., 2013b. Adsorption of Pb²⁺, Cd²⁺, Cu²⁺ and Cr³⁺ onto titanate nanotubes: competition and effect of inorganic ions. *Sci. Total Environ.* 456–457, 171–180.
- Liu, W., Xiao, Z., Wang, T., Zhao, D., Ni, J., 2016. Adsorption of U(VI) by multilayer titanate nanotubes: effects of inorganic cations, carbonate and natural organic matter. *Chem. Eng. J.* 286, 427–435.
- Lu, D., Fang, P., Wu, W., Ding, J., Jiang, L., Zhao, X., Li, C., Yang, M., Li, Y., Wang, D., 2017. Solvothermal-assisted synthesis of self-assembling TiO₂ nanorods on large graphitic carbon nitride sheets with their anti-recombination in the photocatalytic removal of Cr(VI) and rhodamine B under visible light irradiation. *Nanoscale* 9, 3231–3245.
- Luo, J., Sun, M., Ritt, C.L., Liu, X., Pei, Y., Crittenden, J.C., Elimelech, M., 2019. Tuning Pb(II) adsorption from aqueous solutions on ultrathin iron oxychloride (FeOCl) nanosheets. *Environ. Sci. Technol.* 53, 2075–2085.
- Luo, J., Xubiao, L., John, C., Juhui, Q., Yaohui, B., Yue, P., Junhua, L., 2015. Removal of antimonite (Sb(III)) and antimonate (Sb(V)) from aqueous solution using carbon nanofibers that are decorated with zirconium oxide (ZrO₂). *Environ. Sci. Technol.* 49, 11115–11124.
- Nie, Y.-C., Yu, F., Wang, L.-C., Xing, Q.-J., Liu, X., Pei, Y., Zou, J.-P., Dai, W.-L., Li, Y., Suib, S.L., 2018. Photocatalytic degradation of organic pollutants coupled with simultaneous photocatalytic H₂ evolution over graphene quantum dots/Mn-N-TiO₂/g-C₃N₄ composite catalysts: performance and mechanism. *Appl. Catal. B Environ.* 227, 312–321.
- Pi, Y., Li, X., Xia, Q., Wu, J., Li, Y., Xiao, J., Li, Z., 2017. Adsorptive and photocatalytic removal of Persistent Organic Pollutants (POPs) in water by metal-organic frameworks (MOFs). *Chem. Eng. J.* 337, 351–371.
- Qiu, B., Gu, H., Yan, X., Guo, J., Wang, Y., Sun, D., Wang, Q., Khan, M., Zhang, X., Weeks, B., 2014. Cellulose derived magnetic mesoporous carbon nanocomposites with enhanced hexavalent chromium removal. *J. Mater. Chem. 2*, 17454–17462.
- Qiu, J., Zhang, X., Feng, Y., Zhang, X., Wang, H., Yao, J., 2018a. Modified metal-organic frameworks as photocatalysts. *Appl. Catal. B Environ.* 231, 317–342.
- Qiu, J., Zhang, X.F., Zhang, X., Feng, Y., Li, Y., Yang, L., Lu, H., Yao, J., 2018b. Constructing Cd_{0.5}Zn_{0.5}S@ZIF-8 nanocomposites through self-assembly strategy to enhance Cr(VI) photocatalytic reduction. *J. Hazard Mater.* 349, 234–241.
- Ren, Z., Kong, D., Wang, K., Zhang, W., 2014. Preparation and adsorption characteristics of an imprinted polymer for selective removal of Cr(VI) ions from aqueous solutions. *J. Mater. Chem. 2*, 17952–17961.
- Sallem, F., Boudon, J., Heintz, O., Isabelle, S., Megriche, A., Millot, N., 2017. Synthesis and characterization of chitosan-coated titanate nanotubes: towards a new safe nanocarrier. *Dalton Trans.* 46, 15386–15398.
- Song, X.-X., Fu, H., Wang, P., Li, H.-Y., Zhang, Y.-Q., Wang, C.-C., 2018. The selectively fluorescent sensing detection and adsorptive removal of Pb²⁺ with a stable [δ-Mo₂O₂₆]-based hybrid. *J. Colloid Interface Sci.* 532, 598–604.
- Thorne, A., Kruth, A., Tunstall, D., Irvine, J.T., Zhou, W., 2005. Formation, structure, and stability of titanate nanotubes and their proton conductivity. *J. Phys. Chem. B* 109, 5439–5444.
- Wang, C.-C., Yi, X.-H., Wang, P., 2019. Powerful combination of MOFs and C₃N₄ for enhanced photocatalytic performance. *Appl. Catal. B Environ.* 247, 24–48.
- Wang, C.C., Du, X.D., Li, J., Guo, X.X., Wang, P., Zhang, J., 2016. Photocatalytic Cr(VI) reduction in metal-organic frameworks: a mini-review. *Appl. Catal. B Environ.* 193, 198–216.
- Wang, C.C., Li, J.R., Lv, X.L., Zhang, Y.Q., Guo, G., 2014. Photocatalytic organic pollutants degradation in metal-organic frameworks. *Energy Environ. Sci.* 7, 2831–2867.
- Wang, F.X., Yi, X.H., Wang, C.C., Deng, J.G., 2017. Photocatalytic Cr(VI) reduction and organic-pollutant degradation in a stable 2D coordination polymer. *Chin. J. Catal.* 38, 2141–2149.
- Wang, H., Wu, Y., Feng, M., Tu, W., Xiao, T., Xiong, T., Ang, H., Yuan, X., Chew, J.W., 2018. Visible-light-driven removal of tetracycline antibiotics and reclamation of hydrogen energy from natural water matrices and wastewater by polymeric carbon nitride foam. *Water Res.* 144, 215–225.
- Wang, H., Yuan, X., Wu, Y., Zeng, G., Chen, X., Leng, L., Wu, Z., Jiang, L., Li, H., 2015a. Facile synthesis of amino-functionalized titanium metal-organic frameworks and their superior visible-light photocatalytic activity for Cr(VI) reduction. *J. Hazard Mater.* 286, 187–194.
- Wang, H., Yuan, X., Yan, W., Chen, X., Leng, L., Hui, W., Hui, L., Zeng, G., 2015b. Facile synthesis of polypyrrole decorated reduced graphene oxide-Fe₃O₄ magnetic composites and its application for the Cr(VI) removal. *Chem. Eng. J.* 262, 597–606.
- Wang, L., Liu, W., Wang, T., Ni, J., 2013a. Highly efficient adsorption of Cr(VI) from aqueous solutions by amino-functionalized titanate nanotubes. *Chem. Eng. J.* 225, 153–163.
- Wang, T., Liu, W., Xiong, L., Xu, N., Ni, J., 2013b. Influence of pH, ionic strength and humic acid on competitive adsorption of Pb(II), Cd(II) and Cr(III) onto titanate nanotubes. *Chem. Eng. J.* 215–216, 366–374.
- Wang, T., Liu, W., Xu, N., Ni, J., 2013c. Adsorption and desorption of Cd(II) onto titanate nanotubes and efficient regeneration of tubular structures. *J. Hazard Mater.* 250–251, 379–386.
- Wang, X.-L., Zhang, J.-X., Liu, G.-C., Lin, H.-Y., Kang, Z.-H., 2010. Two manganese(II) complexes constructed from 2-(3-pyridyl)-imidazo[4,5-f]1,10-phenanthroline and organic dicarboxylates: syntheses, crystal structures, and luminescence. *J. Coord. Chem.* 63, 3933–3943.
- Wang, X.L., Zhang, J.X., Liu, G.C., Lin, H.Y., Chen, Y.Q., Kang, Z.H., 2011. Effect of flexibility of organic dicarboxylates anions on the four 3D metal-organic frameworks constructed from flexible benzimidazolyl-based ligand. *Inorg. Chim. Acta* 368, 207–215.
- Wu, L., Qiu, Y., Xi, M., Li, X., Cen, C., 2015. Fabrication of TiO₂ nanotubes-assembled hierarchical microspheres with enhanced photocatalytic degradation activity. *New J. Chem.* 39, 4766–4773.
- Wu, Y., Wang, H., Sun, Y., Xiao, T., Tu, W., Yuan, X., Zeng, G., Li, S., Chew, J.W., 2018a. Photogenerated charge transfer via interfacial internal electric field for significantly improved photocatalysis in direct Z-scheme oxygen-doped carbon nitrogen/CoAl-layered double hydroxide heterojunction. *Appl. Catal. B Environ.* 227, 530–540.
- Wu, Y., Wang, H., Tu, W., Liu, Y., Wu, S., Tan, Y.Z., Chew, J.W., 2018b. Construction of hierarchical 2D-2D Zn₃In₂S₆/fluorinated polymeric carbon nitride nanosheets photocatalyst for boosting photocatalytic degradation and hydrogen production performance. *Appl. Catal. B Environ.* 233, 58–69.
- Wu, Y., Wang, H., Tu, W., Wu, S., Liu, Y., Tan, Y.Z., Luo, H., Yuan, X., Chew, J.W., 2018c. Petal-like CdS nanostructures coated with exfoliated sulfur-doped carbon nitride via chemically activated chain termination for enhanced visible-light-driven photocatalytic water purification and H₂ generation. *Appl. Catal. B Environ.* 229, 181–191.
- Wu, Z., Yuan, X., Zeng, G., Jiang, L., Hua, Z., Xie, Y., Hui, W., Chen, X., Hou, W., 2017. Highly efficient photocatalytic activity and mechanism of Yb³⁺/Tm³⁺ codoped In₂S₃ from ultraviolet to near infrared light towards chromium (VI) reduction and rhodamine B oxidative degradation. *Appl. Catal. B Environ.* 225, 8–21.
- Xia, Q., Huang, B., Yuan, X., Wang, H., Wu, Z., Jiang, L., Xiong, T., Zhang, J., Zeng, G., Wang, H., 2018. Modified stannous sulfide nanoparticles with metal-organic framework: toward efficient and enhanced photocatalytic reduction of chromium (VI) under visible light. *J. Colloid Interface Sci.* 530, 481–492.
- Xiong, L., Chen, C., Chen, Q., Ni, J., 2011. Adsorption of Pb(II) and Cd(II) from aqueous solutions using titanate nanotubes prepared via hydrothermal method. *J. Hazard Mater.* 189, 741–748.
- Xiong, L., Ye, Y., Mai, J., Sun, W., Zhang, C., Wei, D., Chen, Q., Ni, J., 2010. Adsorption behavior of methylene blue onto titanate nanotubes. *Chem. Eng. J.* 156, 313–320.
- Xu, C., Liu, H., Li, D., Su, J.H., Jiang, H.L., 2018a. Direct evidence of charge separation in a metal-organic framework: efficient and selective photocatalytic oxidative coupling of amines via charge and energy transfer. *Chem. Sci.* 9, 3152–3158.
- Xu, X.-Y., Chu, C., Fu, H., Du, X.-D., Wang, P., Zheng, W., Wang, C.-C., 2018b. Light-responsive UiO-66-NH₂/Ag₃PO₄ MOF-nanoparticle composites for the capture and release of sulfamethoxazole. *Chem. Eng. J.* 350, 436–444.
- Ye, Y., Shan, C., Zhang, X., Liu, H., Wang, D., Lv, L., Pan, B., 2018. Water decontamination from Cr(III)-Organic complexes based on pyrite/H₂O₂: performance, mechanism, and validation. *Environ. Sci. Technol.* 52, 10657–10664.
- Yi, X.-H., Wang, F.-X., Du, X.-D., Wang, P., Wang, C.-C., 2019. Facile fabrication of BUC-21/g-C₃N₄ composites and their enhanced photocatalytic Cr(VI) reduction performances under simulated sunlight. *Appl. Organomet. Chem.* 33 e4621.
- Yi, X.H., Wang, F.X., Du, X.D., Fu, H., Wang, C.C., 2018. Highly efficient photocatalytic Cr(VI) reduction and organic pollutants degradation of two new bifunctional 2D Cd/Co-based MOFs. *Polyhedron* 152, 216–224.
- Yuan, X., Wang, H., Wang, J., Zeng, G., Chen, X., Wu, Z., Jiang, L., Xiong, T., Zhang, J., Wang, H., 2018. Near-infrared-driven Cr(VI) reduction in aqueous solution based on MoS₂/Sb₂S₃ photocatalyst. *Environ. Sci. Technol.* 8, 1545–1554.
- Zhang, F., Zhang, Y., Zhang, G., Yang, Z., Dionysiou, D.D., Zhu, A., 2018a. Exceptional synergistic enhancement of the photocatalytic activity of SnS₂ by coupling with polyaniline and N-doped reduced graphene oxide. *Appl. Catal. B Environ.* 236, 53–63.
- Zhang, L., Jiang, T., Li, S., Lu, Y., Wang, L., Zhang, X., Wang, D., Xie, T., 2013. Enhancement of photocatalytic H₂ evolution on Zn_{0.8}Cd_{0.2}S loaded with CuS as cocatalyst and its photogenerated charge transfer properties. *Dalton Trans.* 42, 12998–13003.
- Zhang, L., Xia, W., Liu, X., Zhang, W., 2014. Synthesis of titanium cross-linked chitosan composite for efficient adsorption and detoxification of hexavalent chromium from water. *J. Mater. Chem. 3*, 331–340.
- Zhang, S.H., Wu, M.F., Tang, T.T., Xing, Q.J., Peng, C.Q., Li, F., Liu, H., Luo, X.B., Zou, J.P., Min, X.B., 2018b. Mechanism investigation of anoxic Cr(VI) removal by nano zero-valent iron based on XPS analysis in time scale. *Chem. Eng. J.* 335, 945–953.
- Zhao, J., Qiaofeng, H., Junwu, Z., Xiaodong, W., Xin, W., 2014. Synthesis of Bi nanowire networks and their superior photocatalytic activity for Cr(VI) reduction. *Nanoscale* 6, 10062–10070.
- Zhao, X., Cai, Z., Wang, T., O'Reilly, S.E., Liu, W., Zhao, D., 2016a. A new type of cobalt-deposited titanate nanotubes for enhanced photocatalytic degradation of phenanthrene. *Appl. Catal. B Environ.* 187, 134–143.
- Zhao, X., Li, Y., Chang, Z., Chen, L., Bu, X.H., 2016b. A four-fold interpenetrated metal-organic framework as a fluorescent sensor for volatile organic compounds. *Dalton Trans.* 45, 14888–14892.
- Zhao, Y., Parsons, J.G., Peralta-Videa, J.R., Lopez-Moreno, M.L., Gardea-Torresdey, J.L.,

2009. Use of synchrotron- and plasma-based spectroscopic techniques to determine the uptake and biotransformation of chromium(III) and chromium(VI) by *Parkinsonia aculeata*. *Metall* 1, 330–338.
- Zou, J.-P., Chen, Y., Liu, S.-S., Xing, Q.-J., Dong, W.-H., Luo, X.-B., Dai, W.-L., Xiao, X., Luo, J.-M., Crittenden, J., 2019. Electrochemical oxidation and advanced oxidation processes using a 3D hexagonal Co_3O_4 array anode for 4-nitrophenol decomposition coupled with simultaneous CO_2 conversion to liquid fuels via a flower-like CuO cathode. *Water Res.* 150, 330–339.
- Zou, J.-P., Wu, D.-D., Luo, J., Xing, Q.-J., Luo, X.-B., Dong, W.-H., Luo, S.-L., Du, H.-M., Suib, S.L., 2016. A strategy for one-pot conversion of organic pollutants into useful hydrocarbons through coupling photodegradation of MB with photoreduction of CO_2 . *ACS Catal.* 6, 6861–6867.